Check for updates

Indenothiophene-based asymmetric small molecules for organic solar cells†

Qi Shang,‡[ab] Meng Wang,‡[b] Jiajun Wei[bc] and Qingdong Zheng (ID) *[b]

The development of organic semiconductors is of key importance in order to improve the performance of organic solar cells (OSCs). Three indenothiophene (IT)-containing small molecules (**IT3T**, **ITFBT** and **IT2FBT**) were designed and synthesized for small molecule OSCs. The thermal, optical, and electrochemical properties of the molecules were investigated. The optical bandgaps of the three small molecules are ranged from 1.80 to 2.20 eV depending on different terminal groups flanked on the IT. We study the photovoltaic performances of the three molecules by fabricating OSCs with $PC_{71}BM$ as an electron acceptor. Among the three molecules, **ITFBF** exhibited the best power conversion efficiency of 4.57% with a high open circuit voltage (V_{OC}) of 0.98 V. We also briefly discuss structure–property guidelines for small molecules used for OSCs. The results demonstrate that IT-based small molecules are promising for small molecule OSCs with large V_{OC}s.

1. Introduction

Small molecule organic solar cells (OSCs), in which the photo-active layer commonly consists of a p-type semiconducting small molecule and a n-type fullerene derivative, have made significant progress in the past decade.[1–4] In comparison with polymers, semiconducting small molecules for OSCs have the advantages of well-defined structures, high purity, and superior batch-to-batch reproducibility.[5–7] So far, the power conversion efficiency (PCE) of single-junction small molecule OSCs has exceeded 11%.[3]

For small molecule OSCs, the photoactive layer plays an important role not only in the open circuit voltage (V_{OC}), but also in the current density, both of which affect the PCE of the resulting device. Therefore, the innovations in active layer materials are attracting more and more attention. Although a large number of small molecule donors have been used for OSCs, the building blocks for efficient small molecule donors are limited to few symmetric units such as benzodi-thiophene, dithienosilole, indacenedithiophene, and diketo-pyrrolopyrrole.[3,8–11] For example, dithienosilole-based (DTS) derivatives were used for small molecule OSCs as donor units,

leading to PCEs in the range from 5.8% to over 9%.[9] Wang *et al.* introduced indacenedithiophene-based (IDT) derivatives as donor units to produce a series of high performing small molecules for OSCs.[10d] Deng *et al.* reported benzodithiophene-based small molecules with PCEs over 11%.[3] All the small molecules mentioned above have symmetric structures. At the same time, some examples of asymmetric small molecules were also reported for OSCs by Sharma *et al.*[12] However, the number of asymmetric semiconducting molecules is much less than that of the symmetric counterparts due to less availability of asymmetric π-conjugated cores.[4] Recently, our group first introduced asymmetric indenothiophene (IT) to construct donor–acceptor copolymers for polymer solar cells with PCEs over 9%.[13] However, the indenothiophene has never been used for constructing small molecule donors for OSCs.

In this context, three asymmetric indenothiophene-cored small molecules (**IT3T**, **ITFBT** and **IT2FBT**), were designed, synthesized, characterized, and used for the fabrication of OSCs. Three different terminal groups were flanked on the IT core for constructing the target small molecules in order to study the structure–property relationships of the IT-based small molecules. The chemical structures of the target small molecules are shown in Scheme 1. Among them, the devices based on **ITFBT** exhibited the best PCE of 4.57% and a V_{OC} of 0.98 V under AM 1.5 G irradiation (100 mW cm^{-2}). **IT3T** and **IT2FBT** gave low PCEs of 0.71% and 1.92%, respectively.

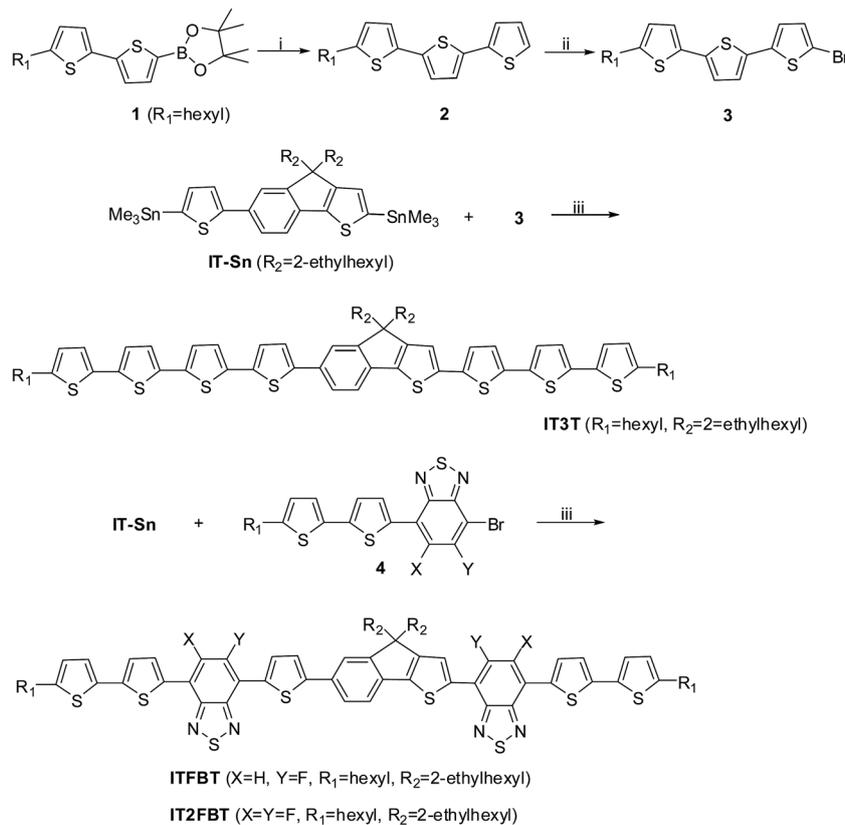*[a]College of Chemistry, Fuzhou University, Fuzhou, 350108, P. R. China*

[b]State Key Laboratory of Structural Chemistry, Fujian Institute of Research on the Structure of Matter, Chinese Academy of Sciences, Fuzhou, 350002, P. R. China. E-mail: qingdongzheng@fjirsm.ac.cn

[c]University of Chinese Academy of Sciences, 19 Yuquan Road, Beijing, 100049, P. R. China

† Electronic supplementary information (ESI) available: Thermogravimetric analysis results, stability of the OSC based on **ITFBT**:$PC_{71}BM$, and the NMR spectra of the small molecules. See DOI: 10.1039/c7ra01902e

‡ These authors contributed equally to this work.

2. Experimental section

2.1 Materials

All reagents were purchased from commercial suppliers, and used as received without further purification unless otherwise

Scheme 1 Synthesis of **IT3T**, **ITFBT** and **IT2FBT**: (i) 2-bromothiophene, Pd$_2$(dba)$_3$, P(o-tolyl)$_3$, aqueous solution, aliquat 336, toluene, reflux, 24 h; (ii) NBS, CH$_2$Cl$_2$, 20 °C; (iii) Pd(PPh$_3$)$_4$, toluene, reflux, 24 h.

stated. Column chromatography was conducted with silica gel (300–400 mesh).

2.2 Synthesis of 5-hexyl-[2,2′;5′,2″]terthiophene (2)[14]

2-(5′-Hexyl-[2,2′-bithiophen]-5-yl)-4,4,5,5-tetramethyl-1,3,2-dioxaborolane (**1**) (2.02 g, 5.4 mmol), 2-bromothiophene (4.34 g, 26.6 mmol), potassium phosphate tribasic (2 M in H$_2$O, 10.0 mmol) and 1 drop of aliquat 336 were added to 50 mL of toluene. After the mixture was degassed, tri(o-tolyl)phosphine (P(o-tol)$_3$) (20 mg, 0.066 mmol) and tris(dibenzylideneacetone) dipalladium(0) (Pd$_2$(dba)$_3$) (10 mg, 0.011 mmol) were added. Then the reaction mixture was stirred vigorously at 110 °C for 24 h. After cooling to room temperature, the mixture was poured into methanol. The crude product was collected by filtration and purified by column chromatography using hexane as eluent to afford compound **2** as a yellow solid (1.06 g, 59%). ^{1}H NMR (CDCl$_3$, 400 MHz, ppm): 7.22 (d, J = 4.8 Hz, 1H), 7.18 (d, J = 3.6 Hz, 1H), 7.08 (d, J = 3.6 Hz, 1H), 7.05–7.00 (m, 3H), 6.71 (d, J = 3.6 Hz, 1H), 2.82 (t, J = 7.6 Hz, 2H), 1.70 (m, 2H), 1.44–1.32 (m, 6H), 0.92 (t, J = 6.8 Hz, 3H).

2.3 Synthesis of 5″-bromo-5-hexyl-[2,2′;5′,2″]terthiophene (3)[14]

N-Bromosuccinimide (NBS) (0.54 g, 3.0 mmol) was added slowly to a solution of compound **2** (1.01 g, 3.0 mmol) in 30 mL of

CH$_2$Cl$_2$. After stirring the mixture at room temperature for 2 h, 10 mL of water was added, and the mixture was then extracted with dichloromethane (2 × 50 mL). The organic phase was washed with water twice, brine solution, then dried over anhydrous MgSO$_4$. After removing the solvent, the crude product was purified by column chromatography to give a yellow solid (0.87 g, 70%). ^{1}H NMR (CDCl$_3$, 400 MHz, ppm): 7.02–6.98 (m, 4H), 6.92 (d, J = 3.6 Hz, 1H), 6.71 (d, J = 3.6 Hz, 1H), 2.81 (t, J = 7.6 Hz, 2H), 1.70 (m, 2H), 1.44–1.31 (m, 6H), 0.92 (t, J = 6.8 Hz, 3H).

2.4 Synthesis of IT3T

Compound **3** (0.50 g, 1.2 mmol), **IT-Sn** (0.33 g, 0.4 mmol) and 20 mL of dry toluene were added into a 50 mL two-neck flask. The solution was degassed by bubbling with nitrogen for 0.5 h. 10 mg of Pd(PPh$_3$)$_4$ was then added and the mixture was heated at 110 °C for 24 h. After the solvent was removed, the crude product was purified by column chromatography to give a red solid (0.31 g, 66%). ^{1}H NMR (CDCl$_3$, 400 MHz, ppm): 7.54 (d, J = 7.6 Hz, 2H), 7.37 (d, J = 8.0 Hz, 1H), 7.27–7.25 (m, 1H), 7.18 (d, J = 3.6 Hz, 1H), 7.14–7.08 (m, 7H), 7.04–7.01 (m, 4H), 6.72 (d, J = 3.6 Hz, 2H), 2.82 (t, J = 7.6 Hz, 4H), 1.99 (br, 4H), 1.75–1.67 (m, 4H), 1.45–1.32 (m, 12H), 1.06–0.85 (m, 22H), 0.79–0.59 (m, 14H); ^{13}C NMR (CDCl$_3$, 100 MHz, ppm): 156.24, 154.04, 154.00, 145.71, 144.12, 140.23, 139.24, 139.22, 139.19, 137.97, 137.10, 137.07, 136.95, 136.26, 136.21, 136.17, 135.90, 135.87, 135.68,

135.30, 135.27, 135.23, 134.46, 130.54, 124.91, 124.76, 124.70, 124.67, 124.63, 124.32, 124.22, 124.15, 123.87, 123.64, 123.48, 123.30, 120.50, 119.03, 54.37, 43.54, 35.06, 34.26, 33.97, 31.65, 30.28, 28.87, 28.59, 27.50, 22.93, 22.67, 14.18, 14.12, 10.74. HRMS (MALDI-DHB, m/z): calcd for $C_{67}H_{78}S_8$ [M]$^+$ 1138.3869; found 1138.3864. Elemental analysis (%) calc. for $C_{67}H_{78}S_8$: C, 70.60; H, 6.90; found: C, 70.41; H, 6.91.

2.5 Synthesis of ITFBT

Following the same procedure as that used for **IT3T**, **ITFBT** was obtained as a dark red solid (0.12 g, 44%) through a Stille coupling reaction between 7-bromo-5-fluoro-4-(5′-hexyl-[2,2′] bithiophenyl-5-yl)-benzo[1,2,5]thiadiazole (0.31 g, 0.6 mmol), and **IT-Sn** (0.17 g, 0.2 mmol). ^{1}H NMR (CDCl$_3$, 400 MHz, ppm): 8.19–8.12 (m, 4H), 7.78–7.67 (m, 3H), 7.64–7.55 (m, 1H), 7.48–7.41 (m, 2H), 7.21–7.17 (m, 2H), 7.13–7.10 (m, 2H), 6.72–6.71 (m, 2H), 2.81 (t, J = 7.2 Hz, 4H), 2.16–2.03 (m, 4H), 1.74–1.67 (m, 2H), 1.42–1.17 (m, 14H), 1.14–0.78 (m, 24H), 0.70–0.61 (m, 12H); ^{13}C NMR (CDCl$_3$, 100 MHz, ppm): 160.17, 157.64, 156.61, 156.60, 154.60, 153.29, 149.67, 147.36, 147.33, 146.08, 143.84, 140.42, 140.37, 140.29, 138.19, 136.91, 134.55, 131.14, 131.08, 131.03, 130.98, 130.86, 129.58, 129.54, 126.23, 126.12, 124.98, 124.94, 123.88, 123.70, 123.23, 123.06, 120.93, 120.91, 119.71, 119.50, 116.17, 115.86, 115.68, 110.85, 110.82, 110.66, 54.53, 43.70, 35.14, 34.10, 34.08, 31.60, 30.26, 28.82, 28.40, 27.53, 22.86, 22.60, 14.15, 14.03, 10.68. HRMS (MALDI-DHB, m/z): calcd for $C_{71}H_{76}F_2N_4S_8$ [M]$^+$ 1278.3804; found 1278.3798. Elemental analysis (%) calc. for $C_{71}H_{76}F_2N_4S_8$: C, 66.63; H, 5.99; N, 4.38; found: C, 66.70; H, 6.12; N, 4.13.

2.6 Synthesis of IT2FBT

Following the same procedure as that used for **IT3T**, **IT2FBT** was obtained a dark red solid (0.14 g, 54%) through a Stille coupling reaction between 4-bromo-5,6-difluoro-7-(5′-hexyl-[2,2′]bithiophenyl-5-yl)-benzo[1,2,5]thiadiazole (0.31 g, 0.6 mmol) and **IT-Sn** (0.16 g, 0.2 mmol). ^{1}H NMR (CDCl$_3$, 400 MHz, ppm): 8.35–8.23 (m, 4H), 7.73–7.70 (m, 2H), 7.56–7.52 (m, 2H), 7.27–7.25 (m, 2H), 7.20–7.17 (m, 2H), 6.79–6.75 (m, 2H), 2.85 (t, J = 7.6 Hz, 4H), 2.20–2.06 (m, 4H), 1.77–1.70 (m, 2H), 1.46–1.23 (m, 14H), 1.10–0.75 (m, 24H), 0.71–0.61 (m, 12H); ^{13}C NMR (CDCl$_3$, 100 MHz, ppm): 155.85, 155.83, 154.83, 150.91, 150.83, 148.75, 148.73, 148.66, 148.60, 148.24, 148.17, 146.45, 145.41, 141.36, 141.28, 141.20, 138.24, 138.20, 134.26, 132.11, 132.09, 132.02, 131.75, 131.71, 131.68, 131.66, 131.59, 131.16, 131.10, 129.97, 129.91, 129.87, 129.83, 126.13, 125.25, 125.05, 124.08, 124.04, 123.14, 120.85, 119.77, 111.21, 54.51, 43.64, 35.16, 34.26, 34.15, 31.65, 30.30, 28.88, 28.40, 27.50, 22.92, 22.66, 14.17, 14.10, 10.75. HRMS (MALDI-DHB, m/z): calcd for $C_{71}H_{74}F_4N_4S_8$ [M]$^+$ 1314.3615; found 1314.3610. Elemental analysis (%) calc. for $C_{71}H_{74}F_4N_4S_8$: C, 64.80; H, 5.67; N, 4.26; found: C, 65.02; H, 5.71; N, 4.19.

2.7 Instruments

^{1}H and ^{13}C NMR spectra were recorded on a Bruker AVANCE-400 spectrometer operating at 400 and 100 MHz, respectively. High-resolution mass spectroscopy (HRMS) measurements were performed on an IonSpec 4.7 T spectrometer. Absorption spectra were obtained by using a spectrophotometer (Lambda 365 UV/vis). The electrochemical cyclic voltammetry measurements were carried out on a CHI 700E electrochemical workstation. OSCs were measured by a Keithley 2440 source measurement unit under AM 1.5 G irradiation (100 mW cm^{-2}) on an Oriel sol3A simulator (Newport) which had been precisely calibrated with a NREL-certified silicon reference cell before testing. The external quantum efficiency (EQE) spectra were measured on a Newport EQE measuring system. Atomic force microscopy (AFM) was performed with the Bruker's Dimension FastScan at a tapping mode.

2.8 Electrochemistry

The cyclic voltammetry (CV) measurements were measured by using a three-electrode cell system (a Pt disk working electrode coated with thin films of small molecules, a Pt wire counter electrode and an Ag/AgNO$_3$ reference electrode). The measurements were performed in a 0.1 mol L^{-1} anhydrous and nitrogen-saturated tetrabutylammonium hexafluorophosphate (Bu$_4$NPF$_6$) acetonitrile solution at a scan rate of 100 mV s^{-1}. The energy level of the ferrocene was assumed to have an absolute energy level of −4.82 eV to vacuum. The highest occupied molecular orbital (HOMO) and the lowest unoccupied molecular orbital (LUMO) energy levels were calculated from the onset oxidation potentials (E_{ox}) and onset reduction potentials (E_{red}) vs. Ag/AgNO$_3$ reference electrode according to the following equations:

$$E_{HOMO} = -(E_{ox} + 4.82) \text{ (eV)}$$

$$E_{LUMO} = -(E_{red} + 4.82) \text{ (eV)}$$

2.9 Fabrication of conventional OSCs

The OSCs were fabricated with the device structure of: indium tin oxide (ITO)/poly(3,4-ethylenedioxythiophene):poly(styrenesulfonate) (PEDOT:PSS)/small-molecule:PC$_{71}$BM/PDIN/Al. ITO glass was cleaned by ultrasonication sequentially in detergent, water, acetone, and isopropanol for 30 min each and then dried in an oven at 80 °C overnight. After the ITO glass substrates were subjected to ultraviolet/ozone treatment for 15 min, PEDOT:PSS (Baytron PVPAI 4083) which had been filtered through a 0.45 μm filter was spin-coated on the ITO substrates at 3000 rpm for 60 s. Then the film-loaded substrates were dried at 140 °C in air for 15 min. A mixture of small-molecule : PC$_{71}$BM (1 : 2.2, w/w) was dissolved in chlorobenzene at a concentration of 20 mg mL^{-1} and stirred overnight. Then the small-molecule : PC$_{71}$BM solution was spin-cast at 1100 rpm for 60 s to form the active layer. An electron injection interlayer was prepared by spin-coating a methanol solution of PDIN (1.5 mg mL^{-1} containing 0.2% acetic acid) to facilitate efficient electron injection. Finally, the negative electrode was prepared by thermally depositing ~120 nm aluminum through a shadow mask under a high vacuum of 5 × 10^{-5} Pa. The device areas of the OSCs were fixed at 0.06 cm^2.

3. Results and discussion

3.1 Synthesis and characterization

The synthetic routes for the target molecules (**IT3T**, **ITFBT** and **IT2FBT**) are shown in Scheme 1 and the detailed synthetic procedures are shown in the Experimental section. The stannylized **IT-Sn** was prepared according to the procedures we reported previously.[13a] The synthesis of compound **3** started from compound **1**, which was reacted with 2-bromothiophene to afford compound **2** in 59% yield. Bromination of compound **2** afforded compound **3** in 70% yield. The Stille reaction between compound **3** and **IT-Sn** using $Pd(PPh_3)_4$ as a catalyst gave compound **IT3T** in 66% yield. Similarly, **ITFBT** and **IT2FBT** were obtained by Stille coupling reactions between **IT-Sn** and the two benzothiadiazole-based bromides **4**, respectively. The chemical structures and the purity of all new compounds were characterized by NMR, elemental analysis and high resolution mass spectrometry (HRMS).

3.2 Thermal properties

The thermal stability of the three small molecules was investigated by thermogravimetric analysis (TGA) at a heating rate of 10 °C min^{-1} under N_2. **IT3T**, **ITFBT** and **IT2FBT** showed sufficiently high decomposition temperatures (T_d) of 403, 405, and 398 °C, respectively (Fig. S1† and Table 1).

3.3 Optical properties

The absorption spectra of **IT3T**, **ITFBT** and **IT2FBT** in solution or in solid state are shown in Fig. 1, and the related parameters are summarized in Table 1. Due to the identical acceptor–donor–acceptor (A–D–A) structured backbone, **ITFBT** and **IT2FBT** exhibited analogous absorption bands both in the solution and in the thin film. For both **ITFBT** and **IT2FBT**, the shorter wavelength absorption bands originate from the π–π* transition and the longer ones are from the intramolecular charge transfer (ICT) between donor and acceptor units. However, **IT3T** exhibited only the π–π* transition band in solution or in thin film, which agrees with the donor–donor configuration of its molecule backbone. In going from the solution to the thin film, the absorption bands of all the three compounds become broadened and red-shifted. However, in comparison with **IT3T**, both **IT2FBT** and **ITFBT** exhibited a more red-shifted absorption in going from solution to thin film indicating a possible stronger π–π interaction for latter
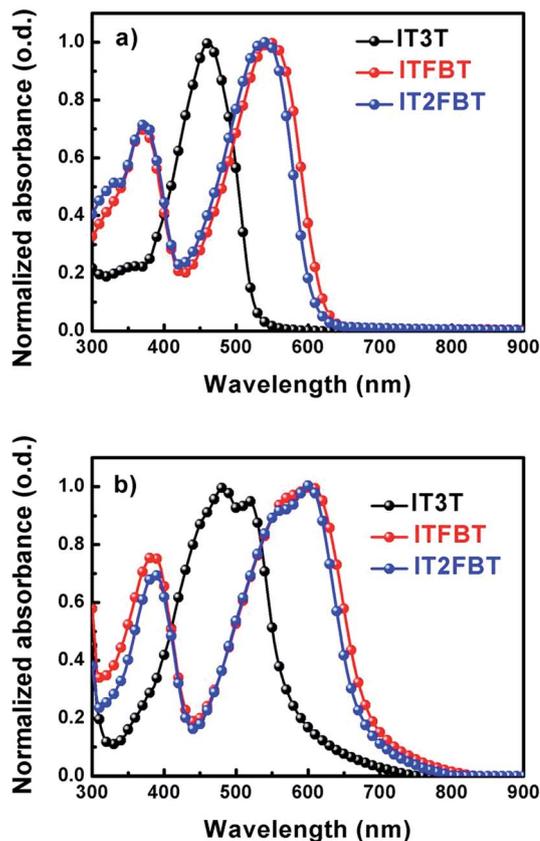

Fig. 1 Normalized absorption spectra of the small molecules in dichloromethane (a) and as-cast films (b).

two. The optical bandgaps of **IT3T**, **ITFBT**, and **IT2FBT** are 2.20, 1.81 and 1.84 eV, respectively. Among the three molecules, **ITFBT** possesses the smallest band gap of 1.81 eV, which is beneficial for enhanced light harvesting.

3.4 Electrochemical properties

To determine the HOMO and the LUMO energy levels of **IT3T**, **ITFBT** and **IT2FBT**, cyclic voltammetry (CV) measurement was performed and the results are shown in Fig. 2 and Table 1. The HOMO energy levels for **IT3T**, **ITFBT** and **IT2FBT** were estimated to be −5.29, −5.35 and −5.46 eV, respectively. Both **ITFBT** and **IT2FBT** exhibit deeper HOMO energy levels in comparison with **IT3T** suggesting that the A–D–A structured backbone is favorable to down-shift the HOMO level of the resulting molecule.

Table 1 Summary of the intrinsic properties of IT3T, ITFBT and IT2FBT

	λ_{max} (nm)		$E_{g,opt}$ (film)[a] (eV)	E_{HOMO} (eV)	E_{LUMO} (eV)	$E_{g,CV}$ (film)[b] (eV)	T_d^c (°C)
	In CH_2Cl_2	Film					
IT3T	525	565	2.20	−5.29	−2.97	2.32	403
ITFBT	621	686	1.81	−5.35	−3.56	1.79	405
IT2FBT	609	673	1.84	−5.46	−3.51	1.95	398

[a] Estimated from the onset of the absorption spectra of thin films. [b] Estimated from cyclic voltammetry. [c] Decomposition temperature at 5% weight loss.
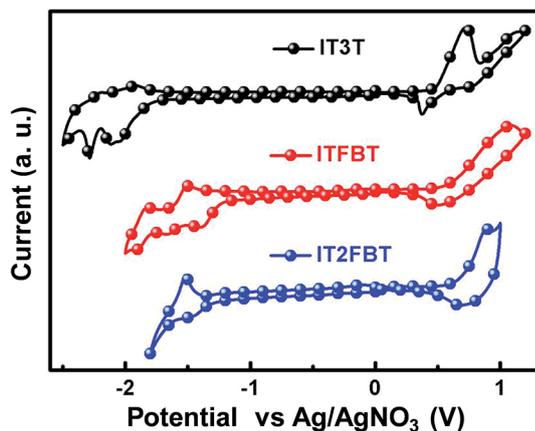
Fig. 2 Cyclic voltammogram of IT3T, ITFBT and IT2FBT thin films.

Compared to **ITFBT**, **IT2FBT** contains two additional electron withdrawing fluorine atoms thereby resulting in a deeper HOMO energy level of −5.46 eV. The electrochemical bandgaps of the three small molecules are also estimated and they share the order of **IT3T** > **IT2FBT** > **ITFBT**, which agrees with their optical bandgap trend. The electrochemical properties of these molecules suggest that molecules with A–D–A structured backbone are beneficial for OSCs with enhanced light absorption as well as large V_{OC}s.

3.5 Photovoltaic performance

The photothose of the voltaic properties of **IT3T**, **ITFBT** and **IT2FBT** were investigated by fabricating OSCs with the device structure of indium tin oxide (ITO)/PEDOT:PSS/donor:PC$_{71}$BM/ PDIN/Al, where PDIN and PEDOT are 2,9-bis(3-(dimethylamino) propyl)anthra[2,1,9-*def*:6,5,10-*d'e'f'*]diisoquinoline-1,3,8,10-(2*H*,9*H*)-tetraone and poly(3,4-ethylenedioxythiophene)/ polystyrene sulfonate, respectively. The best performance OSCs were fabricated by using solutions with a donor (D)/ acceptor (A) ratio of 1 : 2.2 (w/w), and the solutions were spin-coated at a spinning rate of 1100 rpm. The device parameters of all three small molecule-based OSCs are summarized in Table 2. The current density–voltage (J–V) curves of the OSCs are shown in Fig. 3a. It is showed that the OSC based on **ITFBT**:PC$_{71}$BM achieved the best performance among all the three small molecule-based devices. Without any additive, the device based on **ITFBT**:PC$_{71}$BM exhibited a high V_{OC} of 0.98 V, a J_{SC} of 10.24 mA cm^{-2} and a FF of 0.456, all of which leads to a high PCE of 4.57%. With the same A–D–A structured backbone and similar acceptor units, **IT2FBT**-based OSC exhibited

Fig. 3 (a) Current−voltage characteristic of organic solar cells under AM 1.5 G illumination (100 mW cm^{-2}); (b) EQE curves of OSCs; (c) corresponding integrated J_{SC} curves of OSCs.

a lower PCE of 1.92% with a decreased J_{SC} of 6.25 mA cm^{-2}, a reduced FF of 30.5%, but a larger V_{OC} of 1.01 V. The increased V_{OC} is mainly attributed to the deeper HOMO energy level of **IT2FBT** as determined by cyclic voltammogram. However, the device based on **IT3T**:PC$_{71}$BM showed a PCE of 0.71%, with a low J_{SC} of 3.29 mA cm^{-2}, a poor FF of 28.6%, and a low V_{OC} of 0.753 V. The inferior device performance for **IT3T** could be related to its relatively large bandgap, high HOMO energy level, as well as low carrier mobility. It should be noted that these conventional OSCs using PEDOT:PSS as anode buffer layer are relatively unstable over time in ambient conditions (Fig. S2†). However, the shelf stability of OSCs can be greatly enhanced by

Table 2 Device parameters of OSCs based on the small molecules

Compounds	V_{OC} (V)	J_{SC} (mA cm^{-2})	FF (%)	PCE^a (%)
IT3T	0.753	3.29	28.6	0.71 (0.64)
ITFBT	0.979	10.24	45.6	4.57 (4.40)
IT2FBT	1.01	6.25	30.5	1.92 (1.82)

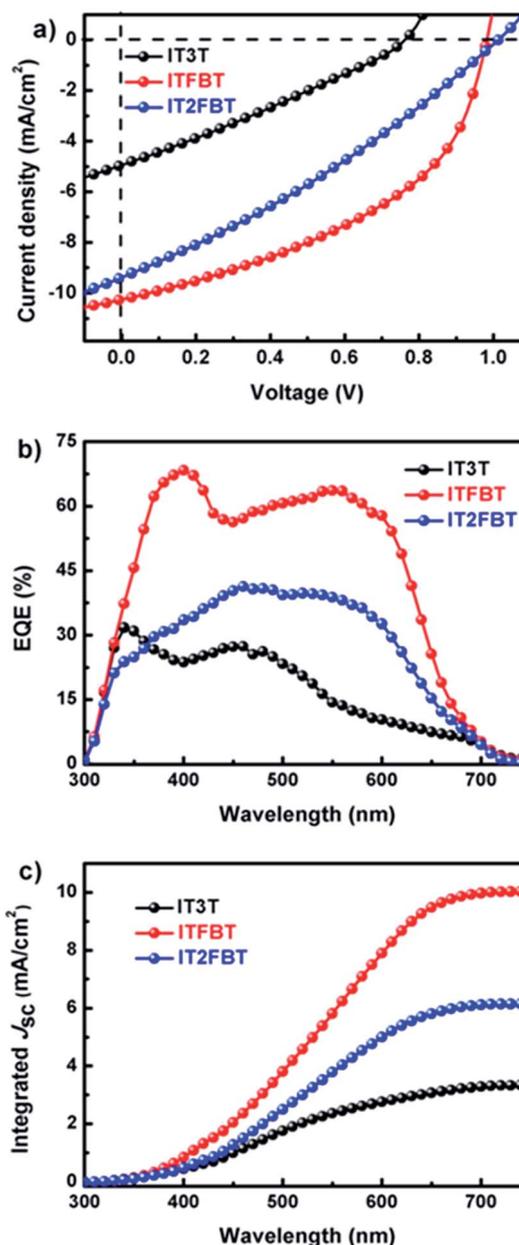^{a} In parentheses are average values based on 8 devices.

adopting an inverted device structure where the PEDOT:PSS is replaced by other inorganic buffer layers.[15] To assure the accuracy of the PCE measurements, external quantum efficiencies (EQEs) of the OSCs were measured and shown in Fig. 3b. All the EQE curves cover a spectral response range from 300 to 700 nm. In this range, the average EQE values of **IT2FBT**- and **ITFBT**-based devices are much higher than those of the **IT3T**-based device. The calculated J_{SC} value from EQE is 10.04 mA cm^{-2} for **ITFBT**, which is very close to that obtained from the J–V measurement (10.24 mA cm^{-2}) within 2% mismatch. The calculated J_{SC} values from the EQE curves of **IT3T**- and **IT2FBT**-based devices are also in agreement with the corresponding measured J_{SC} values. In order to know the origin of the observed photovoltaic performance differences among the three molecules, we measured the hole transport properties of the blend films by using the space charge limited current (SCLC) method. Hole-only devices with the device structure of ITO/PEDOT:PSS/small molecules/MoO$_3$/Au were fabricated. As shown in Fig. 4, **ITFBT** shows the highest hole mobility of 4.8×10^{-4} cm^2 V^{-1} s^{-1} in comparison with **IT3T** (7.9×10^{-6} cm^2 V^{-1} s^{-1}) and **IT2FBT** (8.4×10^{-5} cm^2 V^{-1} s^{-1}). This highest hole mobility of the **ITFBT**-based device explains the higher J_{SC} and improved FF compared to the devices based on the other two molecules.

3.6 Morphology

The surface morphology of the small molecule:PC$_{71}$BM blends was measured by tapping mode atomic force microscopy (AFM). The topography images and corresponding phase images of the small molecule blends are shown in Fig. 5. Among the three topographic images, the **ITFBT**:PC$_{71}$BM film has the most smooth surface, with a small average root mean square (RMS) roughness value of 0.6 nm. While the other two films based on **IT3T**:PC$_{71}$BM and **IT2FBT**:PC$_{71}$BM, have larger RMS roughness values of 1.04 and 1.88 nm, respectively, demonstrating the rougher surfaces than the **ITFBT**:PC$_{71}$BM film. From the phase images, the **ITFBT**:PC$_{71}$BM film shows clear phase seperation features with domain sizes of 10–20 nm. However, the phase seperation features are relatively unclear in the case of
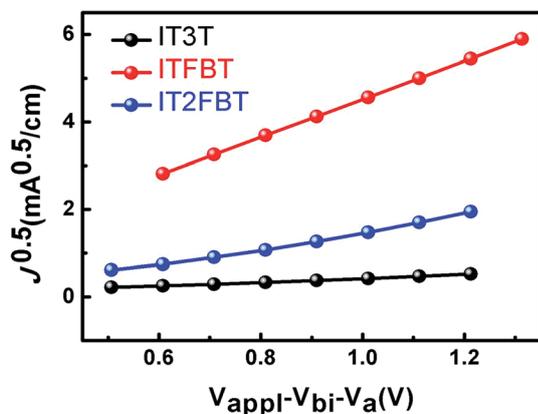

Fig. 5 Tapping mode AFM height (a–c) and phase (d–f) images of IT3T:PC$_{71}$BM, ITFBT:PC$_{71}$BM and IT2FBT:PC$_{71}$BM films, respectively. All the images are 500 × 500 nm.

Fig. 4 $J^{0.5}$–V characteristics of hole-only devices based on IT3T:PC$_{71}$BM blends (~119 nm thickness), ITFBT:PC$_{71}$BM (~101 nm thickness), and IT2FBT:PC$_{71}$BM (~87 nm thickness).
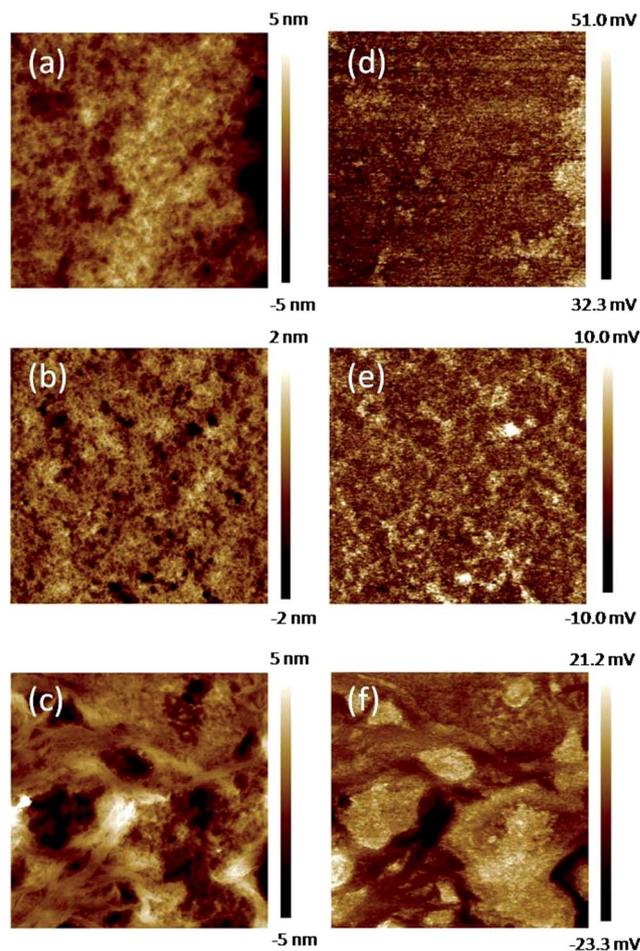
IT3T:PC$_{71}$BM or **IT2FBT**:PC$_{71}$BM. At the same time, apparent aggregates with a domain size of more than 100 nm were found for the **IT2FBT**:PC$_{71}$BM film. This scale is much larger than the exciton diffusion length (<10 nm), leading to an increased recombination rate of the photo-induced excitons before reaching the interfaces. It is believed that nanoscale phase separation enables a large interface area for exciton dissociation and a continuous percolating path for hole and electron transport to the corresponding electrodes.[16] The morphology difference among the three small molecule blends explains the device performance difference for the three molecules with different ending groups.

4. Conclusion

In summary, we designed and synthesized three novel asymmetric small molecules (**IT3T**, **ITFBT** and **IT2FBT**) based on the indenothiophene core. Due to the electron-withdrawing ability of fluorinated benzothiadiazole units, **ITFBT** and **IT2FBT** exhibited deeper HOMO energy levels of −5.35 and −5.46 eV with smaller optical bandgaps (1.81, 1.84 eV), respectively, than those of **IT3T** (−5.29 eV, 2.20 eV), thus leading to the enhanced

photovoltaic performance of **ITFBT** and **IT2FBT**. The best performance device based on **ITFBT** delivered a PCE of 4.57% with a V_{OC} of 0.98 V, a J_{SC} of 10.24 mA cm^{-2} and a FF of 0.456. **IT2FBT** and **IT3T** exhibited relatively lower PCEs of 1.92% and 0.71%, respectively, which can be attributed to the unfavorable energy level, bandgap, carrier mobility or the morphology induced by the difference in their ending groups. The results suggest that the backbone configuration is an important factor determining the performance of the indenothiophene-based small molecules. Nonetheless, our results demonstrate that the asymmetric indenothiophene can be an excellent donor core for small molecule semiconductors.

Acknowledgements

Notes and references

1 Y. Sun, G. C. Welch, W. L. Leong, C. J. Takacs, G. C. Bazan and A. J. Heeger, *Nat. Mater.*, 2012, **11**, 44–48.

2 H. Shang, H. Fan, Y. Liu, W. Hu, Y. Li and X. Zhan, *Adv. Mater.*, 2011, **23**, 1554–1557.

3 D. Deng, Y. Zhang, J. Zhang, Z. Wang, L. Zhu, J. Fang, B. Xia, Z. Wang, K. Lu, W. Ma and Z. Wei, *Nat. Commun.*, 2016, **7**, 13740.

4 Y. Lin, Y. Li and X. Zhan, *Chem. Soc. Rev.*, 2012, **41**, 4245–4272.

5 J. S. Wu, S. W. Cheng, Y. J. Cheng and C. S. Hsu, *Chem. Soc. Rev.*, 2015, **44**, 1113–1154.

6 B. Kan, M. Li, Q. Zhang, F. Liu, X. Wan, Y. Wang, W. Ni, G. Long, X. Yang, H. Feng, Y. Zuo, M. Zhang, F. Huang, Y. Cao, T. P. Russell and Y. Chen, *J. Am. Chem. Soc.*, 2015, **137**, 3886–3893.

7 J.-L. Wang, K.-K. Liu, J. Yan, Z. Wu, F. Liu, F. Xiao, Z.-F. Chang, H.-B. Wu, Y. Cao and T. P. Russell, *J. Am. Chem. Soc.*, 2016, **138**, 7687–7697.

8 (a) J. Zhou, X. Wan, Y. Liu, Y. Zuo, Z. Li, G. He, G. Long, W. Ni, C. X. Li, X. Su and Y. Chen, *J. Am. Chem. Soc.*, 2012, **134**, 16345–16351; (b) P. Dutta, J. Kim, S. H. Eom, W. H. Lee, I. N. Kang and S. H. Lee, *ACS Appl. Mater. Interfaces*, 2012, **4**, 6669–6674; (c) Y. Chen, Z. Du, W. Chen, Q. Liu, L. Sun, M. Sun and R. Yang, *Org. Electron.*, 2014, **15**, 405–413; (d) Z. Wang, X. Xu, Z. Li, K. Feng, K. Li, Y. Li and Q. Peng, *Adv. Electron. Mater.*, 2016, **2**, 1600061.

9 (a) Y. Sun, J. Seifter, L. Huo, Y. Yang, B. B. Y. Hsu, H. Zhou, X. Sun, S. Xiao, L. Jiang and A. J. Heeger, *Adv. Energy Mater.*, 2015, **5**, 1400987; (b) J. Zhou, X. Wan, Y. Liu, G. Long, F. Wang, Z. Li, Y. Zuo, C. Li and Y. Chen, *Chem. Mater.*, 2011, **23**, 4666–4668; (c) A. K. K. Kyaw, D. H. Wang, D. Wynands, J. Zhang, T.-Q. Nguyen, G. C. Bazan and A. J. Heeger, *Nano Lett.*, 2013, **13**, 3796–3801; (d) W. Li, W. Deng, K. Wu, G. Xie, C. Yang, H. Wu and Y. Cao, *J. Mater. Chem. C*, 2016, **4**, 1972–1978; (e) V. Gupta, L. F. Lai, R. Datt, S. Chand, A. J. Heeger, G. C. Bazan and S. P. Singh, *Chem. Commun.*, 2016, **52**, 8596–8599; (f) C. D. Wessendorf, A. Perez-Rodriguez, J. Hanisch, A. P. Arndt, I. Ata, G. L. Schulz, A. Quintilla, P. Bäuerle, U. Lemmer, P. Wochner, E. Ahlswede and E. Barrena, *J. Mater. Chem. A*, 2016, **4**, 2571–2580.

10 (a) W. Yong, M. Zhang, X. Xin, Z. Li, Y. Wu, X. Guo, Z. Yang and J. Hou, *J. Mater. Chem. A*, 2013, **1**, 14214–14220; (b) X. Liu, Q. D. Li, Y. Li, X. Gong, S. J. Su and Y. Cao, *J. Mater. Chem. A*, 2014, **2**, 4004–4013; (c) D. Liu, M. Xiao, Z. Du, Y. Yan, L. Han, V. A. L. Roy, M. Sun, W. Zhu, C. S. Lee and R. Yang, *J. Mater. Chem. C*, 2014, **2**, 7523–7530; (d) J.-L. Wang, F. Xiao, J. Yan, Z. Wu, K.-K. Liu, Z.-F. Chang, R.-B. Zhang, H. Chen, H.-B. Wu and Y. Cao, *Adv. Funct. Mater.*, 2016, **26**, 1803–1812.

11 (a) B. Walker, A. B. Tomayo, X. D. Dang, P. Zalar, J. H. Seo, A. Garcia, M. Tantiwiwat and T. Q. Nguyen, *Adv. Funct. Mater.*, 2009, **19**, 3063–3069; (b) Y. Chen, A. Tang, X. Zhang, Z. Lu, J. Huang, C. Zhan and J. Yao, *J. Mater. Chem. A*, 2014, **2**, 1869–1876; (c) Y. J. Kim, G. B. Lee, C. W. Jeon, Y. H. Kim, D. S. Chung and C. E. Park, *RSC Adv.*, 2015, **5**, 3435–3442; (d) C. H. P. Kumar, K. Ganesh, T. Suresh, A. Sharma, K. Bhanuprakash, G. D. Sharma and M. Chandrasekharam, *RSC Adv.*, 2015, **5**, 93579–93590.

12 (a) T. Jadhav, R. Misra, S. Biswas and G. D. Sharma, *Phys. Chem. Chem. Phys.*, 2015, **17**, 26580–26588; (b) P. Gautam, R. Misra, S. A. Siddiqui and G. D. Sharma, *Org. Electron.*, 2015, **19**, 76–82; (c) P. Gautam, R. Misra, S. A. Siddiqui and G. D. Sharma, *ACS Appl. Mater. Interfaces*, 2015, **7**, 10283–10292; (d) Y. Patil, R. Misra, F. C. Chen, M. L. Keshtov and G. D. Sharma, *RSC Adv.*, 2016, **6**, 99685–99694.

13 (a) M. Wang, D. Cai, Z. Yin, S.-C. Chen, C.-F. Du and Q. Zheng, *Adv. Mater.*, 2016, **28**, 3359–3365; (b) M. Wang, Z. Wang, W. Ma, S.-C. Chen and Q. Zheng, *Adv. Electron. Mater.*, 2016, **2**, 1600340.

14 M. Melucci, G. Barbarella, M. Zambianchi, M. Benzi, F. Biscarini, M. Cavallini, A. Bongini, S. Fabbroni, M. Mazzeo, M. Anni and G. Gigli, *Macromolecules*, 2004, **37**, 5692–5702.

15 Z. Yin, Q. Zheng, S.-C. Chen, D. Cai and Y. Ma, *Adv. Energy Mater.*, 2016, **6**, 1501493.

16 Q. Zheng, B. J. Jung, J. Sun and H. E. Katz, *J. Am. Chem. Soc.*, 2010, **132**, 5394–5404.